

## Title: Photon recycling in lead-iodide perovskite solar cells

**Authors:** Luis M. Pazos-Outón<sup>1</sup>, Monika Szumilo<sup>1</sup>, Robin Lamboll<sup>1,†</sup>, Johannes M. Richter<sup>1,†</sup>, Micaela Crespo-Quesada<sup>2</sup>, Mojtaba Abdi-Jalebi<sup>1</sup>, Harry J. Beeson<sup>1</sup>, Milan Vrucinic<sup>1</sup>, Mejd Alsari<sup>1</sup>, Henry J. Snaith<sup>4</sup>, Bruno Ehrler<sup>3</sup>, Richard H. Friend<sup>1,\*</sup> and Felix Deschler<sup>1,\*</sup>.

† These authors contributed equally to this work.

### Affiliations:

<sup>1</sup>Cavendish Laboratory, University of Cambridge, JJ Thomson Avenue, CB3 0HE, Cambridge, UK

<sup>2</sup>Department of Chemistry, University of Cambridge, CB2 1EW, Cambridge, UK.

<sup>3</sup>FOM Institute AMOLF, Center for Nanophotonics, Science Park 104, 1098 XG Amsterdam, The Netherlands.

<sup>4</sup>Clarendon Laboratory, Department of Physics, University of Oxford, OX1 3PU, Oxford, UK.

\*Correspondence to: [rhf10@cam.ac.uk](mailto:rhf10@cam.ac.uk) and [fd297@cam.ac.uk](mailto:fd297@cam.ac.uk)

### Abstract:

Lead-halide perovskites have emerged as high-performance photovoltaic materials. We mapped the propagation of photogenerated luminescence and charges from a local photoexcitation spot in thin films of lead tri-iodide perovskites. We observed light emission at distances of  $\geq 50$  micrometers and found that the peak of the internal photon spectrum red-shifts from 765 to  $\geq 800$  nanometers. Using a lateral-contact solar cell with selective electron- and hole-collecting contacts, charge extraction for photoexcitation  $> 50$  micrometers away from the contacts was observed that arose from repeated recycling between photons and electron-hole pairs. Thus, energy transport is not limited by diffusive charge transport but can occur over long distances through multiple absorption-diffusion-emission events. This process creates high excitation densities within the perovskite layer, and allows high open circuit voltages.

**Keywords:** Photon recycling, lead-halide perovskites, long-range energy transfer, back-contact solar cell

**One Sentence Summary:** We demonstrate photon recycling in lead iodide perovskite solar cells, which allows for high long charge extraction lengths through multiple absorption-emission events, and contributes to the exceptionally high reported open circuit voltages.

**Main Text:**

Hybrid lead halide perovskite photovoltaics have shown an exceptional rise in power conversion efficiency since their original publication (1) to efficiencies which are almost comparable to crystalline silicon (2–7). This excellent photovoltaic performance has been attributed to well-suited material properties such as high absorption cross-sections (8), long charge carrier lifetimes (9) and high emission yields (10). Recent studies in single crystals have reported charge diffusion lengths of 175  $\mu\text{m}$  (11, 12), and in polycrystalline thin films vertical diffusion lengths have been found to be longer than 1  $\mu\text{m}$  (13, 14). Together with high radiative recombination yields and long carrier lifetimes, these properties raise the question if absorption and reemission of excited carriers can occur during the transport. We report that such ‘photon recycling’ does indeed play a central role, allowing considerable increases over current descriptions in the characteristic lengths for charge and energy transport.

Highly crystalline inorganic semiconductors with high internal quantum yields, such as GaAs, demonstrate the current record efficiencies in single junction solar cells (15, 16). The low non-radiative recombination rates, and high photoluminescence (PL) yields, of these materials allow one photoexcited state to undergo multiple radiative emission-absorption events before it is lost through non-radiative decay (17, 18). This photon recycling effect, together with photonic confinement caused by the difference in refractive index between the active material and its surroundings, leads to a built-up of excited state population in the bulk of the material, similar to a solar concentration effect (17). Additionally, the length scales for energy transport are not limited to a single charge diffusion length, but can occur through multiple recombination-emission events in an interchange between light and charge states, which dramatically enhances the transport length scales.

Previous work on lead iodide perovskites has found a sharp absorption onset at the optical band-edge, with an Urbach Tail slope close to that of GaAs (8, 19), while the PL spectrum is homogeneously broadened by interaction with phonons, leading to a considerable intensity beyond the band-edge (20). Additionally, long carrier lifetimes and low non-radiative losses have been reported (9, 10). These are conditions that could support photon recycling.

We studied thin perovskite films [details of preparation and characterization in the SI (21)] on glass substrates, with a thickness of  $\sim 100$  nm. Under these conditions, only 10 to 15% of internally generated PL escaped to the air above or to the glass below [calculation in the SI (21)], and the remaining emission was guided within the film (22). We measured the spatial distribution of photogenerated emission using a confocal optical microscope setup with separately-controlled excitation and collection objectives and a spatial resolution of  $\sim 1.5$   $\mu\text{m}$  [see Fig. 1A and figure S1 (21)]. Photons propagating in the film could be scattered out of the film or be absorbed and re-emitted isotropically. We measured the emission from the edge of the film, maximizing out-scattering and allowing the detection of both components. These results provide a direct probe of the internal photon distribution traveling through the film. Figure 1B shows spatial emission mapping. When excitation is near the edge ( $\leq 4$   $\mu\text{m}$ ), the observed spectrum is similar to the macroscopic PL of this film, centered  $\sim 765$  nm (cf. Fig. 1C). However, when the excitation objective was moved further away from the collection spot, the internal spectrum continuously red-shifted to beyond 800 nm after the separation increased to 50  $\mu\text{m}$ . Unexpectedly, at these distances, we still detected a blue (765-nm) component in the spectrum at wavelengths similar to the initial emission spectrum, the origin of which we discuss below.

We measured absorption coefficients  $\alpha_\lambda$  of the films using photothermal deflection spectroscopy (PDS), and are compared with photoluminescence excitation spectrum (PLE) in

Fig. 1C. Under conditions where photons are mostly confined within a slab (formed here by the glass/perovskite/air structure) the Beer-Lambert law gives a decay in spectral photon population  $I_\lambda$  away from a point-like excitation spot with radius  $r_0$ :

$$I_\lambda(r) = \frac{r_0}{r} I_{\lambda_0} \cdot e^{-(\alpha_\lambda \cdot r)} \quad (1)$$

This relation indicates that the decay is mono-exponential for each wavelength, with an additional radial factor. Using this equation, the predicted spectral decay map following this law is plotted in Fig. 1D. The measured decay in the different spectral regions was substantially slower than the prediction from the Beer-Lambert law. To illustrate the difference, the decay for selected wavelengths was extracted in Fig. 1E and compared with Beer-Lambert predictions. Beer-Lambert predictions do not take scattering into account, which further accelerates the decay, particularly in spectral regions of very low absorption.

We attribute the main red-shifted peak to guided photons that out-scattered at the edge of the film. Scattering is non-dispersive, thus we expect these to match the internal spectral distribution of photons travelling inside the film. The internal photon spectral distribution was biased towards longer wavelength photons that travelled further between emission and absorption events due to the sharp decay of the absorption coefficient at the band tail. These long wavelength photons were absorbed and generated electron-hole ( $e^-h^+$ ) pairs far from the original excitation spot. When these  $e^-h^+$  pairs recombined, they regenerated the original emission spectrum that peaks near 765 nm, giving rise to the second observed peak. The photon energy gain between absorption and re-emission occurred via phonon-assisted thermalization.

With the observed spatial decay of photon intensity, charges are expected to be generated at comparable distances. To measure the spatial charge distribution directly, we designed a lateral solar cell with  $e^-$  and  $h^+$  selective electrodes. The fabrication process of this back-

contacted device (Fig. 2A) began with a plain sheet of ITO covering a glass substrate. Photolithography was used to make a pattern of ITO with interdigitated electrodes. The channel and electrode width was  $\sim 4 \mu\text{m}$  (a pitch of  $8 \mu\text{m}$ ). Electrodeposition was used to selectively deposit electron- and hole-blocking layers. On half of the electrodes  $\text{TiO}_2$  was deposited from a solution of  $\text{Ti}(\text{O}_2)\text{SO}_4$ , and poly-3,4-ethylenedioxythiophene (PEDOT) from an 3,4-ethylenedioxythiophene (EDOT) monomer-based solution was deposited in the remaining electrode surface. The  $\text{TiO}_2$  layer was formed by hydrolysis, while the PEDOT film formed by polymerization under an external bias. Finally, a layer of perovskite was spin-coated from a standard precursor solution based on methylammonium iodide mixed with lead acetate in DMF (23) and uniform film formation on both electrodes was found. (see experimental section in the SI(21)).

The electric response of this device measured in the dark revealed a diode-like rectifying behavior. Under solar irradiation, a photovoltaic response with an open-circuit voltage of 0.5 V was observed (Figure S14), showing effective carrier selectivity at the electrodes. Photocurrent extraction appeared to be limited compared to vertical solar cells, which may have been caused by energy barriers at the electrodes and an unfavorable charge collection geometry. For comparison, a lateral solar cell without selective layers (Figure S15, (21)) showed a reduced charge selectivity, and very limited voltage and photocurrent.

We used confocal microscopy to map the spatially resolved photocurrent generation in these devices with an excitation resolution below  $1 \mu\text{m}$ . The photocurrent probed the number of photo-excited carriers that reached the electrodes. Figure 2B shows a spatial map of photocurrent both across the interdigitated electrodes ( $\leq 1 \mu\text{m}$ ) and for photoexcitation beyond the electrodes (0 to  $100 \mu\text{m}$ ). The very slow fall-off in photocurrent for excitation

beyond the edge of the electrode structure (see also Fig. 2C) extends well beyond reported diffusion lengths of lead halide perovskite thin films.

In the range of excitation fluences used here, PL in perovskites mainly arises from bimolecular recombination of charge carriers with volume density  $n$ , i.e.  $PL \propto n^2$ , consistent with  $e^-h^+$  recombination (10, 24, 25). Hence, we can relate the locally generated PL, taken around the PL emission peak (765 nm), with the local charge density, and  $\sqrt{PL} \propto n$  is a probe of the spatial charge distribution. Because  $\sqrt{PL}$  decays cylindrically, it must be geometrically corrected by performing a line integral of  $\sqrt{PL}$  over the length of the electrode, in order to compare it with the photocurrent measurements.

In Fig. 2C, we compare the decay of the integrated  $\sqrt{PL}$  with the measured spatial decay of the photocurrent. We observed a similar decay in photocurrent and integrated  $\sqrt{PL}$  beyond 8  $\mu\text{m}$ , which is the resolution set by the electrode geometry. The agreement between these two quantities indicates that the red-shifted component of the recycled photons allows excitation transport over long distances, beyond carrier diffusion lengths, which eventually can be extracted as photocurrent from a solar cell.

To model this, a system of cylindrically symmetric partial differential equations was set up and solved, based on existing theoretical approaches for photon recycling (26–28). We expanded these concepts [full details in the SI, (21)] to take into account local excitation and to calculate the local photon distribution in the film:

$$\frac{dn}{dt} = D\nabla^2 n + G + \frac{c}{n_s} \sum_{\lambda} \alpha_{\lambda} \gamma_{\lambda} - k_1 n - k_2 n^2$$

$$\frac{d\gamma_{\lambda}}{dt} = D_{\lambda} \nabla^2 \gamma_{\lambda} - \frac{c}{n_s} \alpha_{\lambda} \gamma_{\lambda} + (k_2 n^2 P_{stay}) P_{\lambda}$$

The charge carrier concentration  $n$  and the photon density  $\gamma$  were modelled (at different wavelengths  $\lambda$ ) as a function of distance from the excitation spot. Input parameters are reported experimental values for carrier diffusion [diffusion constant  $D = 0.5\text{cm}^2\text{s}^{-1}$ , (9, 11, 12)], mono- and bimolecular recombination of carriers [ $k_1 = 10^6\text{ s}^{-1}$ ,  $k_2 = 10^{-10}\text{ cm}^3\text{s}^{-1}$ , our own measurements and (10, 29)], and the measured wavelength-dependent absorption coefficients  $\alpha_\lambda$  (cf. Fig. 1C). The experimentally measured external bimolecular rate had to be adjusted to take photon recycling into account (30, 31). All absorption of photons is assumed to result in the creation of  $e^-h^+$  pairs, but only the bimolecular channel is radiative, with the spectrum as shown in Fig. 1C, and a proportion  $1-P_{\text{stay}}$  [modelled to be 12.5%, see SI (21)] of these are lost through optical transmission out of the perovskite at the interfaces. The external PL quantum efficiency (PLQE) results from multiple internal recycling events and is related to the internal PLQE by the geometric series:

$$\text{PLQE}_{\text{ext}} = \sum_{r=1}^{\infty} (\text{PLQE}_{\text{int}})^r (1 - P_{\text{escape}})^{r-1} P_{\text{escape}} = \frac{\text{PLQE}_{\text{int}} P_{\text{escape}}}{1 - \text{PLQE}_{\text{int}} (1 - P_{\text{escape}})} \quad (2)$$

The external PLQE varies with distance from the excitation spot and carrier density (Fig. 3A). Photon recycling could be very efficient near the excitation spot, but dropped off at larger distances where charge carrier densities are smaller. From Eq. 2, we find that internal PLQEs can exceed 50% for 1-sun illumination (internal carrier density  $\sim 10^{15}\text{ cm}^{-3}$ ), which correspond to lower measured external PLQEs of  $\sim 10\%$ . The observed recycling effect on extraction would be increased in a solar cell with homogenous illumination, which gives constant carrier densities over the full active area.

In order for this model to match the experimental photocurrent, recycling must be taken into account to explain the observed long spatial decays (Fig. 3B). The model predicts on average one recycling event per photoexcited charge carrier under 1-sun illumination before the carrier decays non-radiatively [calculation in the SI (21)] in a perovskite film in air on glass.

This value relates to a photon recycling-assisted average excitation travel distance of 20  $\mu\text{m}$  (Figure S18). The average travel distance could be enhanced at larger charge densities (for example under high fluences) and can reach values beyond 50  $\mu\text{m}$ .

In terms of  $e^-h^+$  transport, the results suggest that the average distance a charge carrier can travel in perovskites is not limited by the charge carrier diffusion length, for as long as recombination is radiative and the photon stays in the film, the  $e^-h^+$  pair can be regenerated and propagate over large distances. This process creates a distinction between extraction and charge diffusion lengths, and solves the existing contradiction of reported high recombination rates and long ‘diffusion’ lengths.

What are the implications of the observations presented here for standard thin-film perovskite solar cells (3, 6)? The thin-film samples used in our work provide useful model systems for these structures. Using the model and parameters developed above, we estimate that, under open-circuit conditions, in a device with a thickness of 350 nm and non-quenching electrodes, recycling produces a doubling of the internal photon density under 1 sun illumination. These effects can be enhanced even further by minimizing non-radiative decay channels and under higher fluences, such as in solar concentrators, where high bimolecular recombination rates dominate. In the ideal case of unity PLQE and perfect back mirror, photon recycling can produce internal photon densities up to 25 suns ( $4n^2$  with  $n = 2.5$ ) (32) in perovskite solar cells at open circuit. Photon management, such as the use of highly reflective back mirrors to minimize photonic losses and texturing of the top surface, offers promising approaches to use photon recycling to improve photo-conversion efficiencies of perovskite solar cells towards the Shockley-Queisser limit. Higher photon densities lead to higher internal luminescence and to a build-up of excited charges, which increase the split of quasi-Fermi levels and enhance the achievable open circuit voltage in a solar cell.

## References:

1. A. Kojima, K. Teshima, Y. Shirai, T. Miyasaka, Organometal Halide Perovskites as Visible-Light Sensitizers for Photovoltaic Cells. *J. Am. Chem. Soc.* **131**, 6050–6051 (2009).
2. J.-H. Im, C.-R. Lee, J.-W. Lee, S.-W. Park, N.-G. Park, 6.5% Efficient Perovskite Quantum-Dot-Sensitized Solar Cell. *Nanoscale*. **3**, 4088 (2011).
3. M. M. Lee, J. Teuscher, T. Miyasaka, T. N. Murakami, H. J. Snaith, Efficient Hybrid Solar Cells Based on Meso-Superstructured Organometal Halide Perovskite. *Science* **338**, 643–647 (2012).
4. M. Liu, M. B. Johnston, H. J. Snaith, Efficient planar heterojunction perovskite solar cells by vapour deposition. *Nature*. **501**, 395–8 (2013).
5. H.-S. Kim *et al.*, Lead iodide perovskite sensitized all-solid-state submicron thin film mesoscopic solar cell with efficiency exceeding 9%. *Sci. Rep.* **2**, 591 (2012).
6. N. J. Jeon *et al.*, Compositional engineering of perovskite materials for high-performance solar cells. *Nature*. **517**, 476–480 (2015).
7. J. Burschka *et al.*, Sequential deposition as a route to high-performance perovskite-sensitized solar cells. *Nature*. **499**, 316–9 (2013).
8. S. De Wolf *et al.*, Organometallic halide perovskites: Sharp optical absorption edge and its relation to photovoltaic performance. *J. Phys. Chem. Lett.* **5**, 1035–1039 (2014).
9. C. Wehrenfennig, G. E. Eperon, M. B. Johnston, H. J. Snaith, L. M. Herz, High charge carrier mobilities and lifetimes in organolead trihalide perovskites. *Adv. Mater.* **26**, 1584–1589 (2014).
10. F. Deschler *et al.*, High Photoluminescence Efficiency and Optically Pumped Lasing in Solution-Processed Mixed Halide Perovskite Semiconductors. *J. Phys. Chem. Lett.* **5**, 1421–1426 (2014).
11. Q. Dong *et al.*, Electron-hole diffusion lengths > 175 nm in solution-grown CH<sub>3</sub>NH<sub>3</sub>PbI<sub>3</sub> single crystals. *Science*. **347**, 967–970 (2015).
12. D. Shi *et al.*, Low trap-state density and long carrier diffusion in organolead trihalide perovskite single crystals. *Science*. **347**, 519–522 (2015).
13. G. Xing *et al.*, Long-Range Balanced Electron- and Hole-Transport Lengths in Organic-Inorganic CH<sub>3</sub>NH<sub>3</sub>PbI<sub>3</sub>. *Science*, **342**, 344–347 (2013).
14. S. D. Stranks *et al.*, Electron-Hole Diffusion Lengths Exceeding 1 Micrometer in an Organometal Trihalide Perovskite Absorber. *Science* (80-. ). **342**, 341–344 (2013).
15. E. Yablonovitch, O. D. Miller, S. R. Kurtz, in *Conference Record of the IEEE Photovoltaic Specialists Conference IEEE, 2012*, vol. 3, pp. 1556–1559.
16. L. S. Mattos *et al.*, in *Conference Record of the IEEE Photovoltaic Specialists Conference (IEEE, 2012)*; <http://ieeexplore.ieee.org/lpdocs/epic03/wrapper.htm?arnumber=6318255>), pp. 3187–3190.
17. O. D. Miller, E. Yablonovitch, S. R. Kurtz, Strong internal and external luminescence

- as solar cells approach the Shockley-Queisser limit. *IEEE J. Photovoltaics*. **2**, 303–311 (2012).
18. E. Dupont, H. C. Liu, M. Buchanan, S. Chiu, M. Gao, Efficient GaAs light-emitting diodes by photon recycling. *Appl. Phys. Lett.* **76**, 4 (2000).
  19. A. Sadhanala *et al.*, Preparation of Single-Phase Films of  $\text{CH}_3\text{NH}_3\text{Pb}(\text{I}_{1-x}\text{Br}_x)_3$  with Sharp Optical Band Edges. *J. Phys. Chem. Lett.* **5**, 2501–2505 (2014).
  20. C. Wehrenfennig, M. Liu, H. J. Snaith, M. B. Johnston, L. M. Herz, Homogeneous Emission Line Broadening in the Organo Lead Halide Perovskite  $\text{CH}_3\text{NH}_3\text{PbI}_{3-x}\text{Cl}_x$ . *J. Phys. Chem. Lett.* **5**, 1300–1306 (2014).
  21. full details can be found online in Supplementary Information.
  22. I. Suárez, E. J. Juárez-Pérez, J. Bisquert, I. Mora-Seró, J. P. Martínez-Pastor, Polymer/Perovskite Amplifying Waveguides for Active Hybrid Silicon Photonics. *Adv. Mater.* **27** (2015)
  23. W. Zhang *et al.*, Ultrasmooth organic-inorganic perovskite thin-film formation and crystallization for efficient planar heterojunction solar cells. *Nat Commun.* **6**, 6142 (2015).
  24. Y. Yamada, T. Nakamura, M. Endo, A. Wakamiya, Y. Kanemitsu, Photocarrier Recombination Dynamics in Perovskite  $\text{CH}_3\text{NH}_3\text{PbI}_3$  for Solar Cell Applications. *J. Am. Chem. Soc.* **136**, 11610–11613 (2014).
  25. L. M. Herz, Charge Carrier Dynamics in Organic-Inorganic Metal Halide Perovskites. *Annu. Rev. Phys. Chem.* **in press** (2016).
  26. J. L. Balenzategui, A. Martí, Detailed modelling of photon recycling: Application to GaAs solar cells. *Sol. Energy Mater. Sol. Cells.* **90**, 1068–1088 (2006).
  27. S. M. Durbin, J. L. Gray, Numerical modeling of photon recycling in solar cells. *IEEE Trans. Electron Devices.* **41**, 239–245 (1994).
  28. R. Graaff, J. J. Ten Bosch, Diffusion coefficient in photon diffusion theory. *Opt. Lett.* **25**, 43 (2000).
  29. M. B. Johnston, L. M. Herz, Hybrid Perovskites for Photovoltaics: Charge-Carrier Recombination, Diffusion, and Radiative Efficiencies. *Acc. Chem. Res.*, acs.accounts.5b00411 (2015).
  30. R. K. Ahrenkiel *et al.*, Ultralong minority-carrier lifetime epitaxial GaAs by photon recycling. *Appl. Phys. Lett.* **55**, 1088–1090 (1989).
  31. P. Renaud *et al.*, Influence of photon recycling on lifetime and diffusion coefficient in GaAs. *J. Appl. Phys.* **71**, 1907–1913 (1992).
  32. Q. Lin *et al.*, Electro-optics of perovskite solar cells. *Nat. Photonics.* **9**, 106–112 (2014).

**Acknowledgments:** The authors acknowledge financial support from the Engineering and Physical Sciences Research Council of the UK (EPSRC) and King Abdulaziz City for Science and Technology (KACST). L.M.P.O. and H.J.B. also thank the Nano doctoral training center (NanoDTC) for financial support. M.S., M.V. and J.M.R. thank the Winton

programme for the physics of sustainability. M.C.Q would like to thank the Marie Curie Actions (FP7-PEOPLE-IEF2013) for funding. M.A.J. thanks Nyak Technology Ltd for PhD scholarship and B.E. acknowledges the Foundation for Fundamental Research on Matter (FOM), which is part of the Netherlands Organization for Scientific Research (NWO). F.D. acknowledges funding through a Herchel Smith Research Fellowship. We acknowledge Prof. Henning Sirringhaus, Prof. Neil Greenham, Prof. Ullrich Steiner, Dr. Erwin Reisner and Prof. Richard Phillips for providing support and access to their facilities.

Supplementary Material with references 33- 49 and full data can be found online.

# Figures:

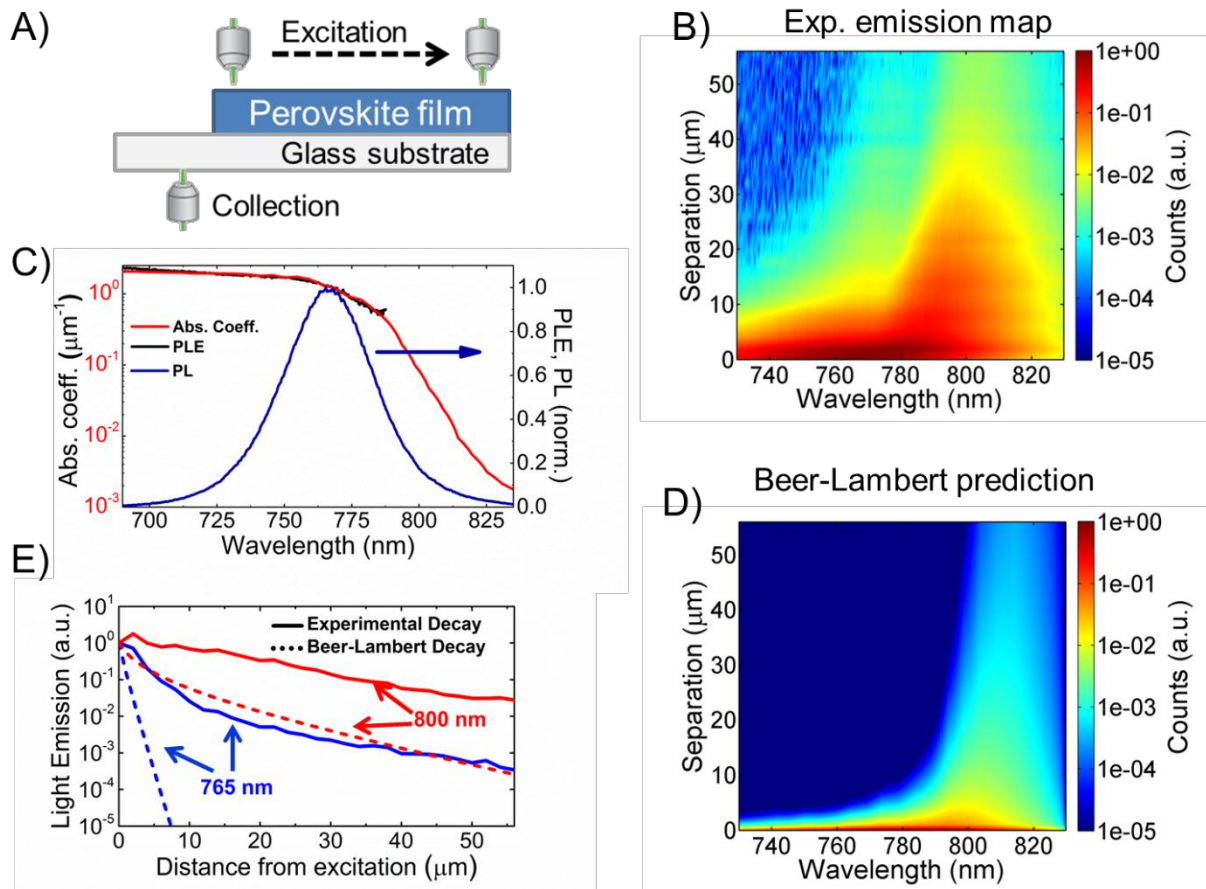


**Fig. 1.** Spatial mapping of emission and photon spectrum. (A) Graphical representation of microscope setup and measurement geometry. (B) Experimentally measured light emission map for different separation distances between excitation and collection. (C) Comparison of PL with PL excitation (PLE) and photothermal deflection spectra (PDS). (D) Predicted spatial light emission spectra from cylindrically decaying Beer-Lambert law. (E) Comparison between experiment (solid lines) and expected decay (broken lines) from the Beer-Lambert law at 765 and 800 nm. The experimental data is not in agreement with simple linear absorption, which suggests that additional processes, such as photon recycling, maintain substantial photon intensity at large distances.

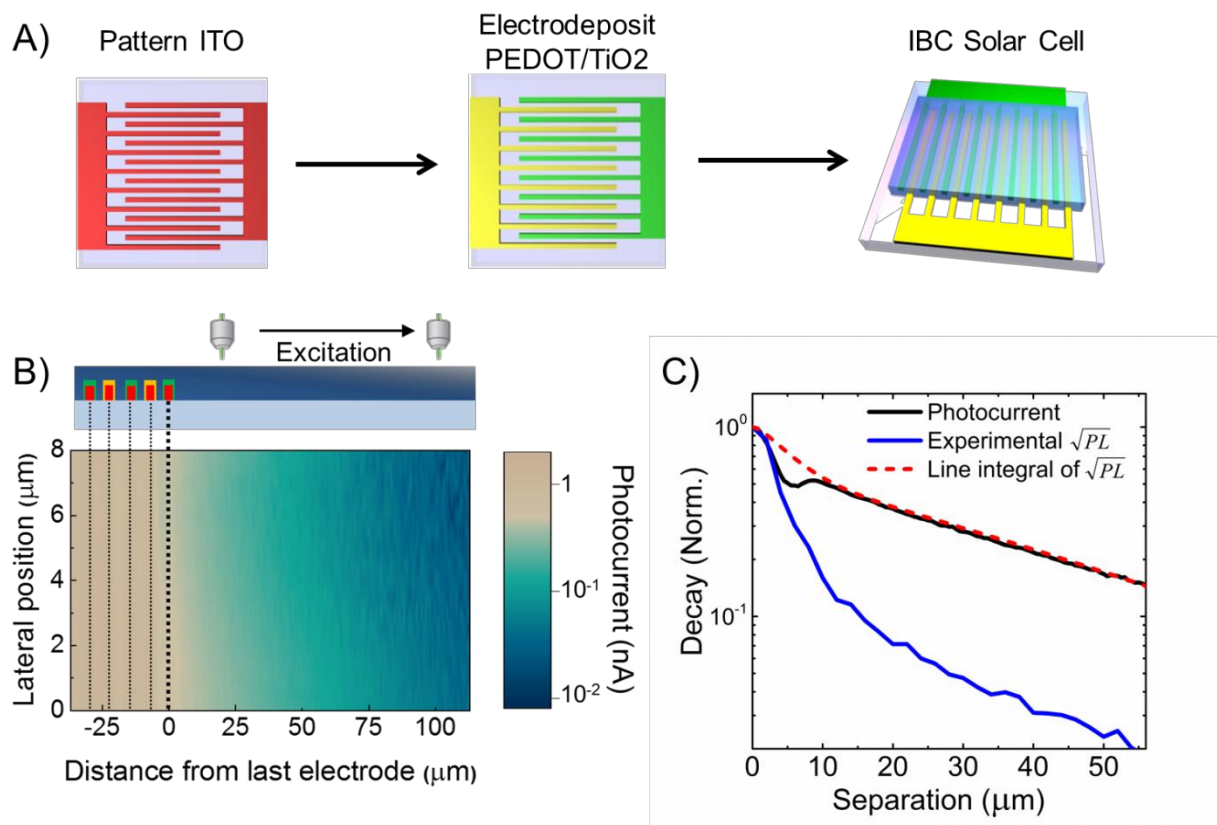


**Fig. 2.** Photocurrent mapping of an interdigitated back contact (IBC) perovskite solar cell. A) Fabrication process of IBC device: pattern a flat sheet of ITO, electrodeposit TiO<sub>2</sub> on half the fingers and PEDOT on the other half, spincoat the photoactive perovskite layer. B) Photocurrent map at the edge of the active area of an IBC perovskite device. Lateral position along the electrode direction. We observed photocurrent several tens of microns beyond the last electrode (x-axis position 0 μm, bold dashed line) C) Comparison between spatial decay of photocurrent and square root of PL. These results suggest that photon densities, which propagate over large distances through the material assisted by photon recycling, can be extracted as photocurrent.

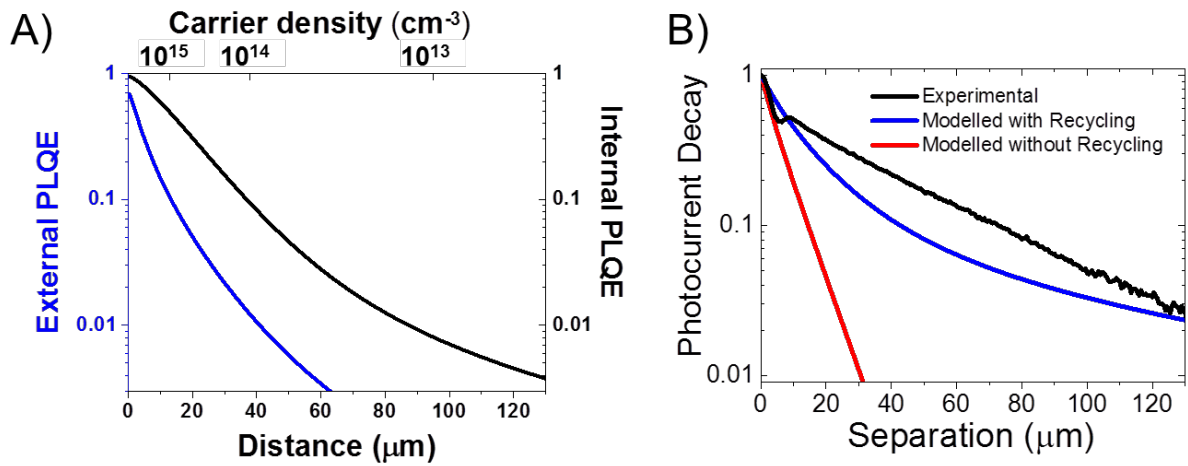


**Fig. 3.** A) Change in external and internal photoluminescence quantum efficiency (PLQE) as a function of distance derived from a photon recycling diffusion model as presented in the text, with reported mono- and bimolecular recombination ( $k_{\text{mono}} = 10^6 \text{ s}^{-1}$ ,  $k_{\text{bi}} = 10^{-10} \text{ cm}^3 \text{ s}^{-1}$ ) and diffusion constants ( $D = 0.5 \text{ cm}^2 \text{ s}^{-1}$ ) of photoexcited carriers. B) Predicted spatial photocurrent decay for the model with and without photon recycling.